AGU ADVANCING EARTH AND SPACE SCIENCES

Geophysical Research Letters

RESEARCH LETTER
10.1029/2023GL104829

Typical Synoptic Patterns Responsible for Summer Regional Hourly Extreme Precipitation Events Over the Middle and Lower Yangtze River Basin, China

Jingwen Zeng[1], Anning Huang[1], Peili Wu[2], Danqing Huang[1], Yan Zhang[3,4], Jian Tang[5], Dajun Zhao[6], Ben Yang[1], and Shuang Chen[1]

[1]School of Atmospheric Sciences, Frontiers Science Center for Critical Earth Material Cycling, Nanjing University, Nanjing, China, [2]Met Office Hadley Centre, Exeter, UK, [3]Key Laboratory of Radiometric Calibration and Validation for Environmental Satellites, National Satellite Meteorological Center, China Meteorological Administration (LRCVES/CMA), Beijing, China, [4]FengYun Meteorological Satellite Innovation Center (FY-MSIC), Beijing, China, [5]National Meteorological Center of China Meteorological Administration, Beijing, China, [6]State Key Laboratory of Severe Weather, Chinese Academy of Meteorological Sciences, Beijing, China

Abstract Based on the hourly rainfall gauge data and ERA5 reanalysis for the period 1980–2020, typical synoptic patterns responsible for summer regional hourly extreme precipitation events (RHEPE) over the middle and lower Yangtze River basin have been objectively identified using a circulation clustering method. It is found that the Meiyu front with different locations and intensities imbedded in the East Asian summer monsoon, and landfalling typhoons are the leading contributors. As the dominant synoptic pattern, the Meiyu front pattern is associated with ~92% of the total RHEPE occurrence and can be categorized into a southerly strong-Meiyu type and a northerly weak-Meiyu type. The RHEPE occurrence shows a predominant morning peak associated with the southerly strong-Meiyu type and a secondary late afternoon peak related to the northerly weak-Meiyu type, in which the Meiyu front is pushed northward by the strengthened western North Pacific subtropical high accompanied by accelerated low-level southwesterly flow.

Plain Language Summary Using ERA5 reanalysis and hourly gauge rainfall measurements in summers of 1980–2020, this study investigates the driving mechanisms and temporal variation of summer regional hourly extreme rainfall events over the middle and lower Yangtze River basin. Typical synoptic patterns responsible for the summer regional hourly rainfall extremes are objectively identified using spectral clustering analysis. The Meiyu front with different locations and intensities imbedded in East Asian summer monsoon and the landfalling typhoons are the synoptic patterns leading to the regional hourly rainfall extremes. The diurnal twin peaks (morning and late afternoon) in the occurrence of regional hourly rainfall extremes are related to the Meiyu front with different locations and intensities. The results from this investigation may help improve the prediction and climate risk assessment of regional extreme rainfall events.

Key Points:

- The Meiyu front imbedded in the East Asian summer monsoon and landfalling typhoons are the leading contributors of summer regional hourly extreme precipitation events (RHEPE) over middle and lower Yangtze River basin
- The Meiyu front pattern can be sorted into a southerly type with strong Meiyu front and a northerly type with weak Meiyu front
- The northerly weak Meiyu front pattern with active convection contributes the most to the afternoon diurnal peak of RHEPE occurrence

Supporting Information:

Supporting Information may be found in the online version of this article.

Correspondence to:

A. Huang and D. Huang,
anhuang@nju.edu.cn;
huangdq@nju.edu.cn

Citation:

Zeng, J., Huang, A., Wu, P., Huang, D., Zhang, Y., Tang, J., et al. (2023). Typical synoptic patterns responsible for summer regional hourly extreme precipitation events over the middle and lower Yangtze River basin, China. *Geophysical Research Letters*, *50*, e2023GL104829. https://doi.org/10.1029/2023GL104829

Received 6 JUN 2023
Accepted 22 AUG 2023

Author Contributions:

Conceptualization: Anning Huang
Data curation: Jingwen Zeng, Anning Huang, Jian Tang, Ben Yang, Shuang Chen
Formal analysis: Jingwen Zeng, Anning Huang, Danqing Huang
Investigation: Jingwen Zeng, Peili Wu, Danqing Huang, Yan Zhang, Dajun Zhao, Ben Yang

1. Introduction

Extreme precipitation (EP) often leads to disastrous impacts on human society and economy, and easily result in flash floods (D. Gu, 2019; W. Zhang & Zhou, 2020). Under the influence of global warming, both the frequency and intensity of EP are increasing across the world in both dry and wet regions (Donat et al., 2016; Kamae et al., 2021; Prein et al., 2017; Ren et al., 2021; B. Sun et al., 2021; Q. Sun et al., 2021). Rising temperatures increase the moisture holding capacity of the atmosphere, which is an exponential function of temperature governed by the Clausius-Clapeyron relation (Allen & Ingram, 2002; O'Gorman & Muller, 2010; van de Vyver et al., 2019). Increased moisture supply from the atmosphere provides the potential for the occurrence of EP. As global warming, the risk of both occurrence and potential damages from EP is projected to increase further (W. Zhang et al., 2021).

Due to the lack of high-resolution observations and inaccurate model simulations, there are huge uncertainties in the description and future climate projections of EP, although efforts have been made to reduce such uncertainties (Thackeray et al., 2022). However, the prediction of EP is still a big challenge due to the complexity of related circulation and the rapidness of EP development. Numerous studies have been conducted to improve the prediction skills of EP. Besides improving the numerical simulation skills by increasing model spatial and

Methodology: Jingwen Zeng, Anning Huang
Resources: Jingwen Zeng, Anning Huang, Yan Zhang, Jian Tang
Software: Jingwen Zeng, Shuang Chen
Supervision: Anning Huang, Danqing Huang
Validation: Jingwen Zeng, Peili Wu, Dajun Zhao, Shuang Chen
Visualization: Jingwen Zeng
Writing – original draft: Jingwen Zeng, Anning Huang
Writing – review & editing: Jingwen Zeng, Anning Huang, Peili Wu, Danqing Huang, Yan Zhang, Dajun Zhao, Ben Yang

temporal resolutions, developing parameterization schemes and so on (Hui et al., 2015; Lin et al., 2019; N. Luo & Guo, 2021; Luu et al., 2022; C. Zhao et al., 2019), the recently populated machine learning methods have also been applied to seek improvement of EP prediction through related synoptic pattern analysis (Gottardi et al., 2012; Nayak & Ghosh, 2013; Nguyen-Le & Yamada, 2019; Nguyen-Le et al., 2017). Based on synoptic situations, the hourly EP records in China are divided into four kinds: the tropical cyclone, surface front, vortex/shear line, and weak-synoptic forcing (Y. Luo et al., 2016). An agglomerative hierarchical clustering was also applied to classify the large-scale circulation responsible for the regional EP over the middle reaches of Yangtze River (Y. Hu et al., 2019).

The middle and lower Yangtze River basin (MLYRB) is one of the most prosperous economic centers in China, possessing abundant hydrological resources and inevitably a high risk of disastrous EP (H. Gu et al., 2015). The regional EP in MLYRB mostly happens in summer and is largely influenced by the East Asian summer monsoon (EASM), especially the associated Meiyu front (Ding, 2004; Ding & Chan, 2005; Ng et al., 2021). Previous studies have indicated that the EP in MLYRB generally associates to the strengthened and westward-extended western North Pacific subtropical high (WNPSH) accompanied by the intensified and eastward-extended South Asian high (SAH) (Tang et al., 2021; F. Tian et al., 2022; Y. Tian et al., 2022; Q. Zhang et al., 2017; Y. Zhao et al., 2020).

The strong influence of EP is mainly due to its rapid development and strong temporal and spatial locality. Therefore, detailed investigation of EP based on hourly precipitation data is rather important (X. Li et al., 2022). Recent studies have shown that the summer EP in MLYRB displays significant diurnal variation, exhibiting two diurnal peaks with one in late afternoon and the other in morning. The morning peak is generally caused by large-scale weather systems dominated by dynamic processes, while the afternoon precipitation peak is usually influenced by local-scale weather systems, which are mainly controlled by the thermodynamic processes (Xue et al., 2018; A. Q. Zhang et al., 2020; Y. Zhao et al., 2020). As EP is resulted from synoptic systems with different spatial-temporal scales, it can be sorted into regional/synoptic-scale and local-scale events according to Ng et al. (2021), who have shown that changes of EP over eastern China in the warm season during 1970–2019 mainly came from the regional scale, which can lead to more severe social and economic impacts due to its larger coverage and longer duration compared to the local-scale.

However, the lack of high-resolution data has restricted previous synoptic analysis of regional EP mostly to daily and semidiurnal scale, which is not precise enough to represent the detailed characteristics of EP at much shorter time scale, such as hourly scale. In addition, several studies have pointed out that the hourly EP is more sensitive to the temperature change and increase at a faster rate than that on the daily scale (Kendon et al., 2018; Wei et al., 2013; Wood & Ludwig, 2020; Xiao et al., 2016). Therefore, based on hourly precipitation and atmospheric reanalysis fields, here we aim to identify and clarify the synoptic patterns responsible for the summer regional hourly EP event (RHEPE) in MLYRB, and focus on the issues below: (a) What are the typical synoptic patterns responsible for the RHEPE occurrences? (b) What are the characteristics of each synoptic pattern? (c) What are the physical processes and mechanisms related to the synoptic patterns?

2. Data and Methods

2.1. Precipitation Data and Reanalysis Data

The data used in current study are listed as follows:

1. The hourly rain gauged precipitation data at 308 stations over MLYRB in summer (June, July, and August) during 1980–2020, which are collected and qualified by the China Meteorology Administration.
2. The geopotential height, zonal, meridional wind, specific humidity and convective available potential energy (CAPE) data of the ERA5 reanalysis (Hersbach et al., 2020) with the temporal resolution of 1 hr and the horizontal resolution of 0.25° during 1980–2020, which are available at https://cds.climate.copernicus.eu/cdsapp#!/dataset/reanalysis-era5-pressure-levels.

2.2. Methodology

Based on hourly summer precipitation data of 1980–2020, the 95th percentile threshold of all the historical rainfall records with the intensity ≥0.1 mm at each station is first calculated, and then the EP is detected as the hourly

precipitation amount exceeds the 95th percentile threshold for each station at a given time, where the 95th percentile threshold is defined as the value ranking at the 95% when ordering the total record to ascending order. Similarly, the number of stations with simultaneous EP is first counted at each hour in the summers of 1980–2020, and then the RHEPE is detected when the number of stations (≥1) with simultaneous EP occurrence exceeds the 95th percentile threshold of the counted station numbers within a specific region at a given time (Tang et al., 2021; Xie et al., 2018). Based on the methods mentioned above, we detected 2,283 hr of RHEPE over MLYRB during the summers of 1980–2020, which contributes 2.52% of the total hours in summers of 1980–2020.

Spectral clustering is then applied to classify the synoptic patterns during RHEPEs over MLYRB in summer. It helps us overcome two major problems in clustering: one is the shape of cluster and the other is the cluster centroid. K-means algorithm generally assumes that the clusters are spherical or round, that is, within k-radius from the cluster centroid. In K-means, many iterations are required to determine the cluster centroid. In spectral clustering, the clusters do not follow a fixed shape or pattern. Points that are far away but connected belong to the same cluster and the points which are less distant from each other could belong to different clusters if they are not connected. This implies that the algorithm could be effective for data of different shapes and sizes (von Luxburg, 2007; Tripathy et al., 2021).

We first select the u and v components of wind at 1,000, 850, 500, and 200 hPa during RHEPE and normalize the time series at each grid in the MLYRB region (112°–123°E, 28°–34°N). Then we flatten the spatial dimensions (level: 4, latitude: 28 and longitude: 48) into a one-dimensional array ($4 \times 28 \times 48 = 5{,}376$) for each case of time when RHEPE happens and put the v array after u array to form the whole spatial array with the size of 10,752 ($5{,}376 \times 2$) (Tang et al., 2021). For the 2283 hr of RHEPE, a two-dimensional array (temporal: 2,283, spatial: 10,752) is formed to be the input data of spectral clustering. In determination of the number of cluster groups, we consider both the Calinski-Harabasz score and the physical condition to divide the samples into three clusters (Figures S1 and S2 in Supporting Information S1).

Since the precipitation data does not conform the normal distribution and the significance of long-term trends is not suitable to be tested by t-test, the Mann-Kendall test, a non-parametric test, is chosen to examine the significance of trends in different clusters (Gocic & Trajkovic, 2013).

Meiyu front is a quasi-stationary front embedded in the EASM that brings continuous rainy days to eastern China (He et al., 2007; Ninomiya, 2000), the position of Meiyu front is determined by the maximal meridional gradient of potential pseudo-equivalent temperature at 850 hPa within the belt with the intensity $\geq 10\ \mathrm{k} \cdot 100\ \mathrm{km}^{-1}$ (Figures S3a and S3b in Supporting Information S1) (Gao et al., 2020; Y. Hu et al., 2021; Huang et al., 2011; Ninomiya, 1984, 2000).

3. Results

3.1. Background

The RHEPE contributes more than 20% of the total EP (including local and regional EP events) amount and occurrence frequency along the MLYRB with much larger contribution near the estuary (Figures 1a and 1b), which are the sensitive regions. Moreover, the contribution of RHEPE to the total EP amount and occurrence at most sites (more than 90% of the total stations) in the MLYRB show increasing trends during the past 40 years despite that most trends are not significant at 0.05 significance level (Figures 1c and 1d). And the clustering result show that the increasing trend is mostly contributed by the landfalling typhoons (significant at 0.05 significance level) and the synoptic pattern 1 (not significant) (Figure S4 in Supporting Information S1).

3.2. Dominant Synoptic Patterns

Figures 2a–2c shows the typical synoptic patterns during the RHEPE at 200, 500, and 850 hPa, the synoptic patterns 1 and 2 lead to about 92% of the total occurrence of RHEPE over the MLYRB in summer, both are featured by the EASM with a strong and eastward-extended SAH at 200 hPa (Figures S5a and S5d in Supporting Information S1), a strengthened western North Pacific Subtropical High (WNPSH) at 500 hPa (Figures S5b and S5e in Supporting Information S1) and a strong low-level southwesterly jet at 850 hPa over the MLYRB (Figures 2a and 2b), corresponding to previous study (Q. Zhang et al., 2017). From Figures 2a and 2b, it can be noted that the synoptic patterns 1 and 2 are both featured by a Meiyu front imbedded in the EASM but with

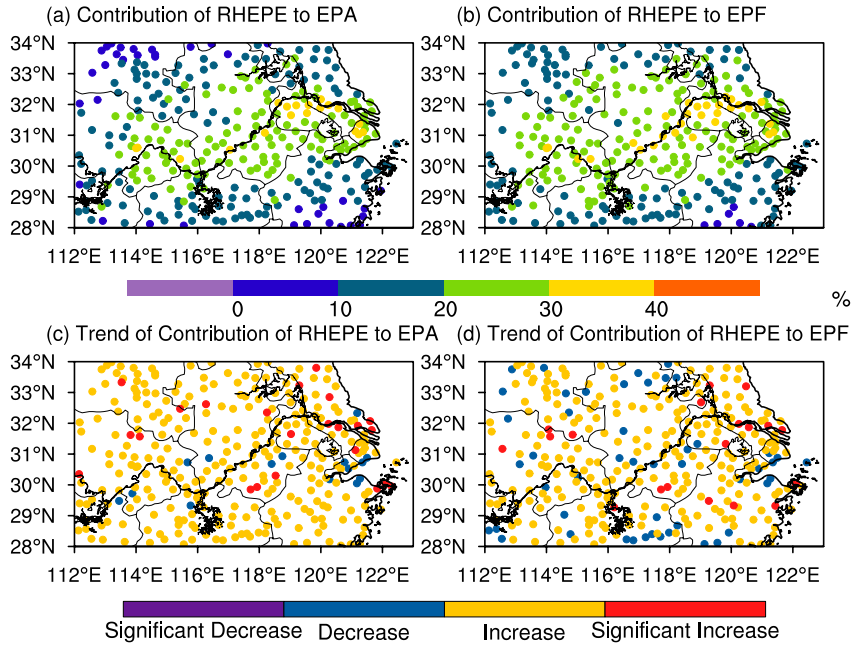

Figure 1. The contribution of regional hourly extreme precipitation events to the total Extreme precipitation (EP) (local and regional EP) amount (EPA) (a), occurrence frequency (EPF) (b), trends of the contribution in (a) and (b) are show in (c) and (d), respectively. The significance of trends in (c) and (d) is tested by the Mann-Kendall trend test, and the significant increase/decrease trend is at the 0.05 significance level.

different locations and intensities. Compared to pattern 2, the Meiyu front in synoptic pattern 1 is located farther south and much stronger (Figures S3a and S3b in Supporting Information S1) with relatively stronger southwesterly wind over southern MLYRB and relatively stronger northerly wind over northern MLYRB (Figures S4c and S4f in Supporting Information S1). The synoptic pattern 3 is apparently dominated by the landfalling typhoons which result in about 8% of the total RHEPE occurrences (Figure 2c).

Figures 2d–2f show the configuration of the climatology and controlling synoptic patterns of RHEPE at different levels. The WNPSH (SAH) is anomalously strong over the south of MLYRB at 500 hPa (200 hPa) under the synoptic patterns 1 and 2 (Figures S5b and S5e in Supporting Information S1), and locates farther west (east) compared to the climatology (Figures 2d and 2e). The strengthened WNPSH at 500 hPa accompanied by the intensified and eastward-extended SAH at 200 hPa are responsible for the RHEPE associated with a Meiyu front imbedded in the EASM. The sub-seasonal variation of the RHEPE occurrence under the three synoptic patterns is further shown in Figures 2g–2i. Clearly, the RHEPEs under pattern 1 mostly occur in June, and the RHEPEs under pattern 2 and 3 mostly occur in July and August, respectively.

3.3. Moisture Supply

We further investigate the moisture supply under each synoptic pattern. All the three synoptic patterns present a strong moisture convergence (Figures 3d–3f) over the regions with relatively higher occurrence probability of EP. The moisture supply under the synoptic patterns 1 and 2 are both carried by the accelerated low-level southwesterly jet from the South China Sea and the Bay of Bengal (Figures 3a and 3b), while the moisture transport and convergence are much stronger in pattern 1 (Figures 3a and 3d) than in pattern 2 (Figures 3b and 3e). Unlike the other 2 synoptic patterns, the water vapor under the landfalling typhoon pattern is transported from the South and East China Sea, and the strongest moisture convergence is located over the coastal region (Figures 3c and 3f), corresponding to the EP with much higher occurrence probability (Figures 2c and 2f).

3.4. Diurnal Variability

As shown in Figure 4a, the total RHEPE occurrences show double diurnal peaks with a predominant peak in morning (8:00 LST) and a secondary peak in late afternoon (17:00 LST), this is consistent with previous studies

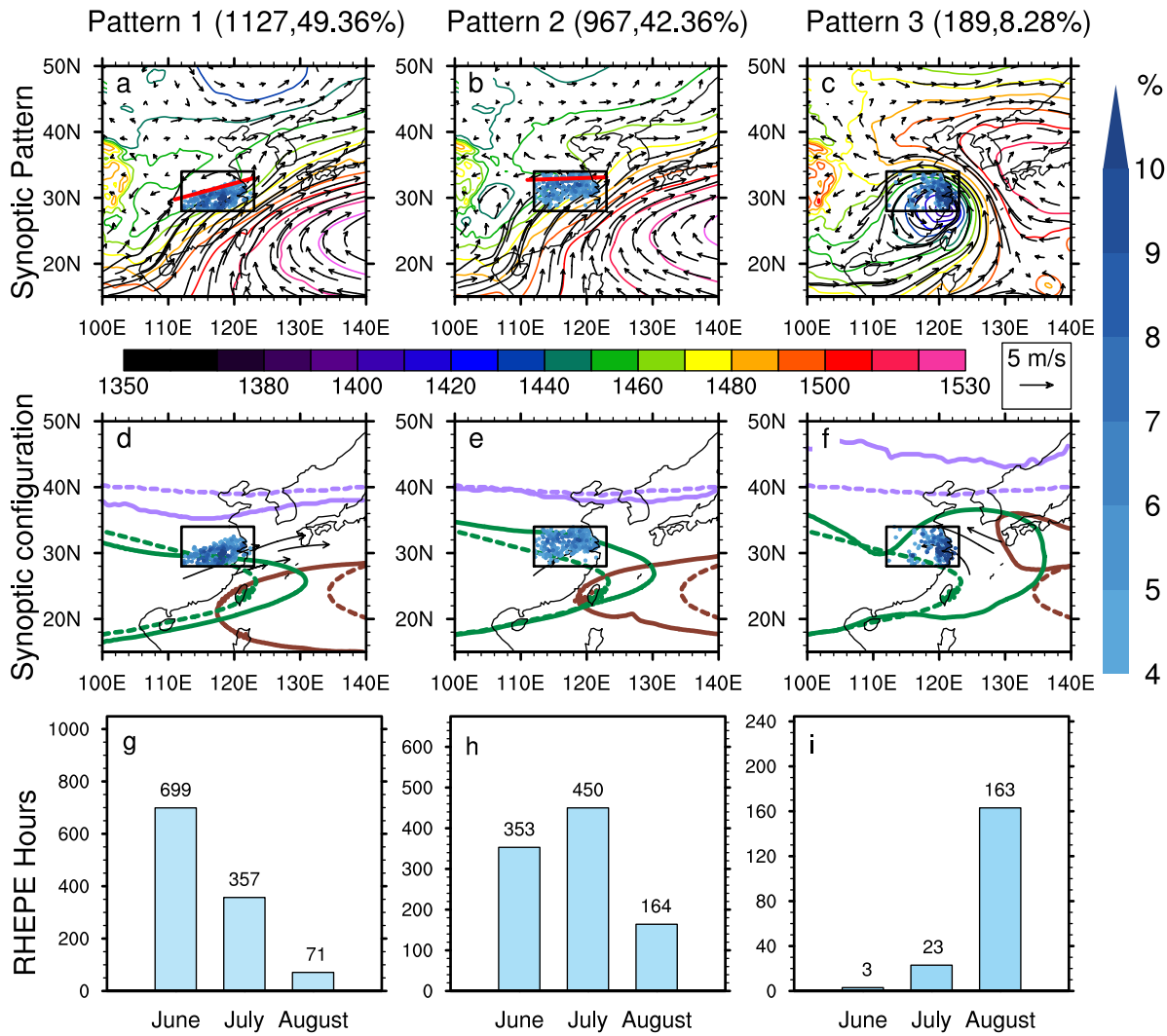

Figure 2. The typical synoptic patterns at 850 hPa responsible for the summer regional hourly extreme precipitation events (RHEPE) over the middle and lower Yangtze River basin (a–c). The contour lines (arrows) show the composite mean geopotential height (wind fields) during the RHEPE, and the blue dots indicate the occurrence probability of Extreme precipitation (EP) (right color bar), which is defined as the ratio of total EP occurrences at a given site under a given synoptic pattern to the total occurrences of this synoptic pattern. The red lines indicate the position of Meiyu front in (a, b). Configuration of South Asian high (SAH) at 200 hPa (solid green lines), western North Pacific subtropical high (WNPSH) at 500 hPa (solid brown lines), and the wind anomalies at 850 hPa under each synoptic pattern (d–f). Dashed (solid) green lines represent the SAH indicated by the 12,500 gpm contour at 200 hPa and dashed (solid) brown lines indicate the WNPSH indicated by the 5,880 gpm contour at 500 hPa in the climatology of 1980–2020 (composite mean under each synoptic pattern). The vectors in (d–f) indicate the anomalous winds at 850 hPa under each synoptic pattern relative to the climatic mean in summers of 1980–2020. The RHEPE occurrences (units: hour) under different synoptic patterns in June, July, and August during the summers of 1980–2020 (g–i).

(Jiang et al., 2020; Xue et al., 2018), while the landfalling typhoon pattern contributes much less to the total diurnal variation of RHEPE occurrence than the other 2 synoptic patterns. Under the synoptic pattern 1 (2), the diurnal variation of RHEPE occurrence exhibits a morning peak (two peaks with a dominant one in late afternoon and a secondary one in early morning). The morning peak caused by the synoptic pattern 1 is mostly controlled by the boundary layer inertial oscillation, which triggers the nocturnal low-level southwesterly jet and enhances moisture supply and wind convergence in early morning (Chen et al., 2009; Du & Chen, 2018; H. Li et al., 2018; Xue et al., 2018). On the other hand, the major peak in late afternoon corresponding to the synoptic pattern 2 is mainly resulted from the afternoon surface heating under the influence of the strengthened WNPSH, leading to more convective precipitation (Yang & Smith, 2006). To understand the convective activities, we further investigate the convective nature of each synoptic pattern through the convective available potential energy (CAPE). As shown in Figure 4b, the diurnal variation of CAPE shows a single peak in the afternoon for all the three synoptic patterns, indicating the afternoon surface heating process. Meanwhile, the CAPE over the MLYRB is much

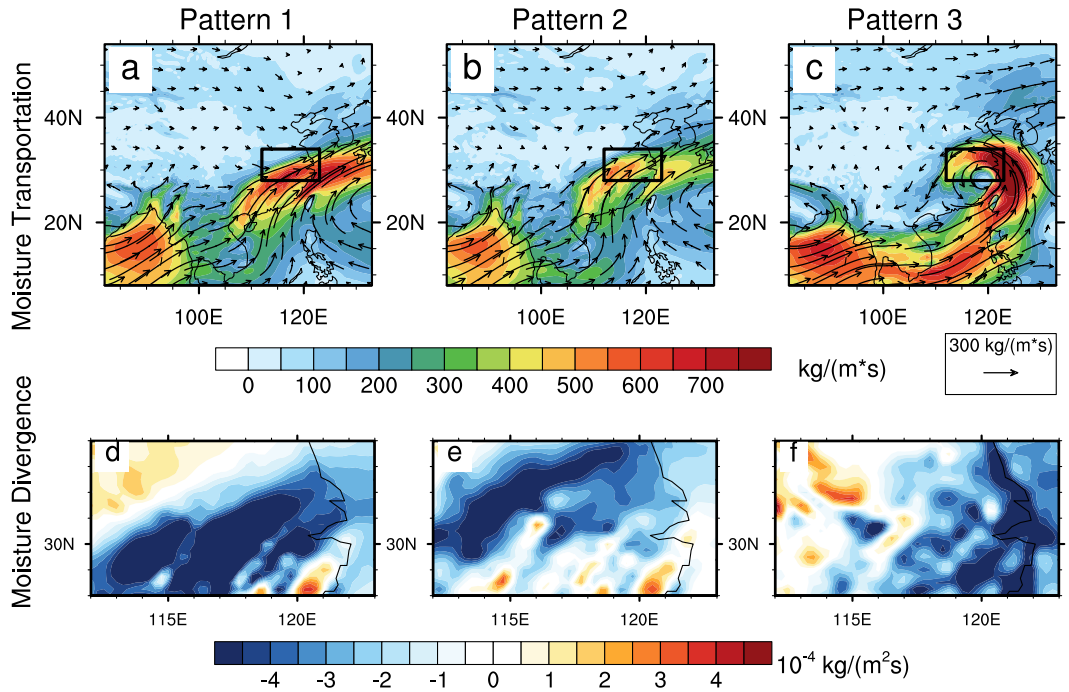

Figure 3. (a–c) The column-integrated (surface to 300 hPa) moisture transport flux (vector) and magnitude (shadings). (d–f) The column-integrated (surface to 300 hPa) divergence of moisture transport flux.

stronger in the synoptic pattern 2 than in the other two synoptic patterns (Figures 4c–4f), implying much stronger convective activities under the synoptic pattern 2 relative to the other two synoptic patterns.

3.5. Development of Atmospheric Circulations Before the RHEPE

As shown in Figures 5c–5e, during the 24 hr before the RHEPE under the synoptic pattern 1, an anomalous cyclone over the MLYRB and surrounding areas at 850 hPa develops and strengthens with the Meiyu front transitioned from an east-west strike to a southwest-northeast strike due to the strengthened northeasterly winds over the northwest of MLYRB, and the stratiform precipitation induced by the Meiyu front (A. Q. Zhang et al., 2020) takes longer time to develop into RHEPE than that under the synoptic pattern 2 (Figures S6b and S6d in Supporting Information S1). Similar to the situations under the synoptic pattern 1, an anomalous cyclone appears over the MLYRB and surrounding areas at 12 hr before the RHEPE and strengthens in the following 12 hr under the synoptic pattern 2. In addition, the quasi-easterly wind anomaly over the north of MLYRB along the north edge of anomalous cyclone intensifies and the Meiyu front keeps steady east-west strike during the development of RHEPE under the synoptic pattern 2 (Figures 5h–5j). Meanwhile, it is clear that it takes shorter time to develop into RHEPE (Figures 5a–5j) and the duration is much shorter for RHEPE (Figures S6b and S6d in Supporting Information S1) under the synoptic pattern 2 than those under the pattern 1. This short-duration RHEPE is well corresponding to the nature of convective precipitation under the synoptic pattern 2 (Figure 4e) (Berg & Haerter, 2013). Under the landfalling typhoon pattern, the RHEPE develops with the landfalling process of typhoon, first occurs in the coastal areas during 24 to 12 hr before RHEPE and quickens as the typhoon eye reaches the land (Figures 5k–5o).

Among the three synoptic patterns, the mean EP intensity over MLYRB induced by the synoptic pattern 2 (3) is the strongest (weakest) in most hours before the RHEPEs (Figure S5a in Supporting Information S1), which cover the least (most) number of stations (Figure S5c in Supporting Information S1) and show the shortest (longest) duration under the synoptic pattern 2 (3) (Figures S5b and S5d in Supporting Information S1). This also supports that the RHEPEs under the synoptic pattern 2 are mostly dominated by the convective precipitation induced by local thermodynamic processes with much shorter development time and smaller coverage area (X. Hu et al., 2022; Y. Luo et al., 2013), while the RHEPEs caused by the landfalling typhoons (pattern 3) are

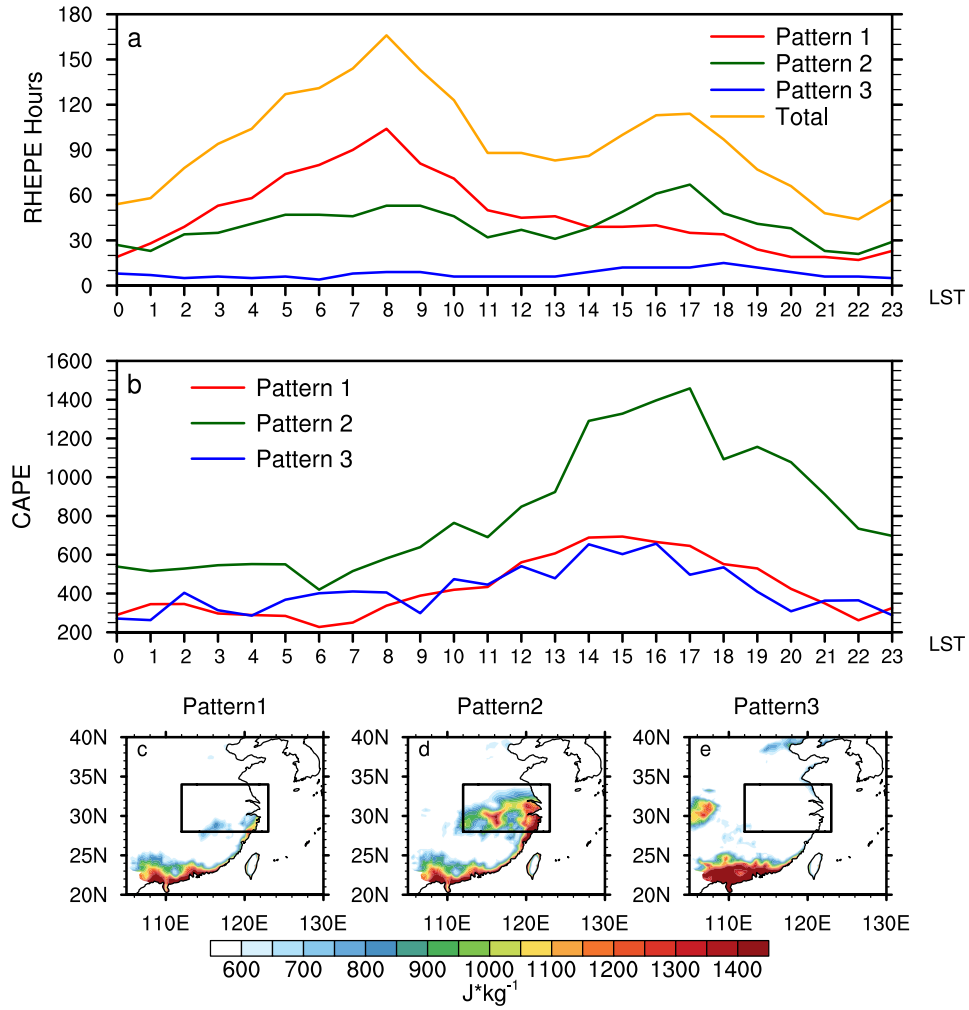

Figure 4. The diurnal variation of the regional hourly extreme precipitation events (RHEPE) occurrence (a) and regionally averaged convective available potential energy (CAPE) (b) over the middle and lower Yangtze River basin (28°N–34°N, 112°E–122°E) in summer under different synoptic patterns; mean CAPE during the RHEPEs under each synoptic pattern (c–e).

featured by relatively persistent moderate-intensity precipitation with much longer life time and larger coverage area (Figures S5b, S5c, and S5d in Supporting Information S1).

4. Conclusions

Recently, Tang et al. (2021) have revealed the dominant synoptic patterns for the summer regional EP events over the lower MLYRB based on the 12-hourly data. However, the time scale of the datasets is coarse to investigate the detailed features, such as the diurnal cycle of the RHEPE, which is important for understanding the formation mechanisms of regional EP events. Therefore, in this study, the hourly precipitation data is applied to indicate the hourly behavior of RHEPE over the MLYRB. This study identifies the typical synoptic patterns responsible for the summer RHEPE over the MLYRB using hourly rainfall observations and ERA5 reanalysis during 1980–2020. The main findings are listed as follows:

There are two major dynamic drivers of summer RHEPE in the MLYRB. One is related to a Meiyu front with different locations and intensities imbedded in the EASM and the other is related to the landfalling typhoons. The former (later) accounts for about 92% (8%) of the total occurrence of RHEPE. The synoptic pattern with a Meiyu front imbedded in the EASM can be further divided into two sub-categories: a southerly type with strong Meiyu front accompanied by an obvious westerly trough at 200–500 hPa (pattern 1) and a northerly type with weak Meiyu front (pattern 2) imbedded in the EASM (Figures S3 and S4a–S4f in Supporting Information S1),

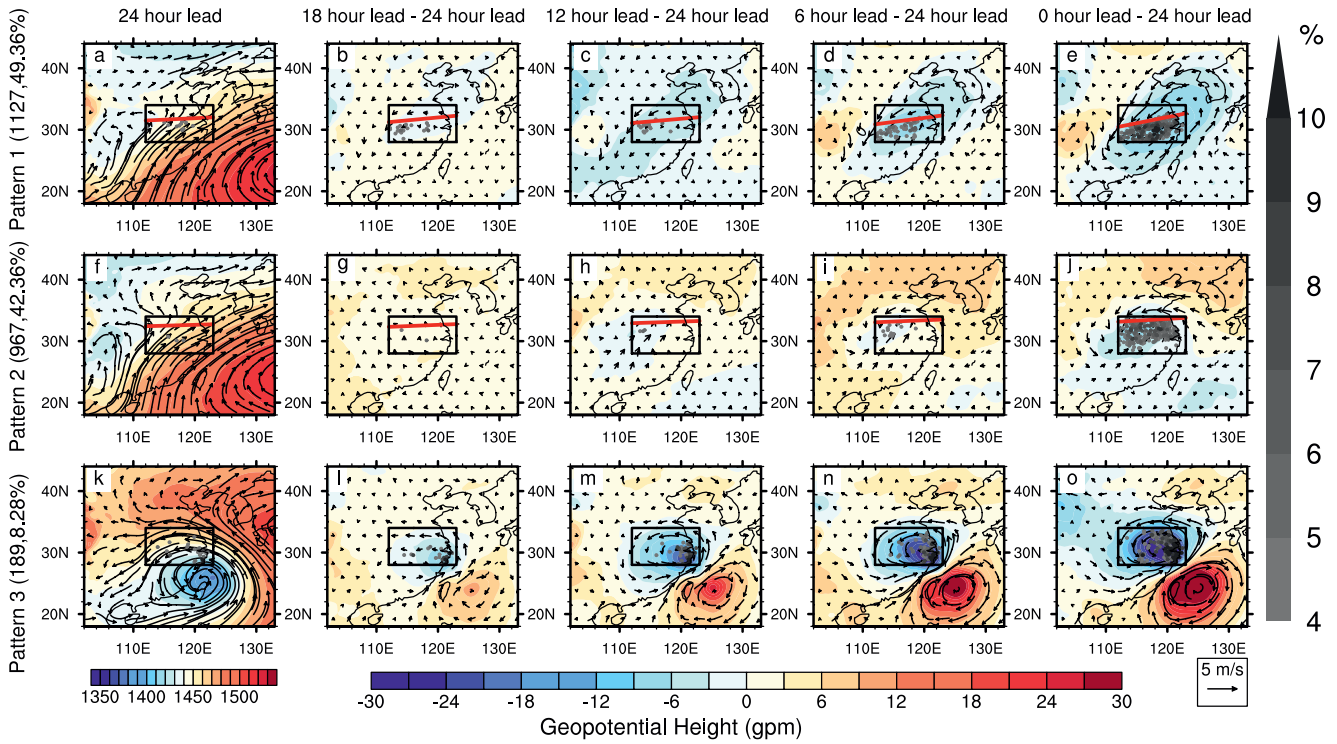

Figure 5. The composite mean atmospheric circulation at the 24 hr before the regional hourly extreme precipitation events (RHEPE) under each synoptic pattern (a, f, and k) and the changes in the atmospheric circulation relative to that at the 24 hr before the RHEPEs under each synoptic pattern (b–e, g–j, and l–o). The contour shadings (arrows) show the composite mean geopotential height and its changes indicated by bottom color bar (wind fields) at 850 hPa, and the gray dots indicate the occurrence probability of Extreme precipitation (EP) (right color bar), which is defined as the ratio of total EP occurrences at a given site under a given synoptic pattern to the total occurrences of this synoptic pattern. The red lines in a-j indicate the position of Meiyu front.

they contribute 49.36% and 42.36% of the total RHEPE occurrences in summer over the MLYRB, respectively. Meanwhile, the high EP occurrence probability induced the synoptic pattern 1 (2) is concentrated in the southern (northern) MLYRB.

There is a clear double-peak diurnal cycle in the occurrence of summer RHEPE over the MLYRB with an early morning one around 08:00 LST and a late afternoon one around 17:00 LST. The early morning peak is predominantly driven by the synoptic pattern 1 with a strong Meiyu front located south (Xue et al., 2018; A. Q. Zhang et al., 2020) and the late afternoon peak is resulted from the synoptic pattern 2 featured by a farther north located weak Meiyu front imbedded in EASM. Corresponding to the diurnal cycle, the mean EP intensity is the largest (lowest) for RHEPEs under the synoptic pattern 2 (pattern 3, landfalling typhoon pattern). The RHEPEs induced by the synoptic pattern 2 (landfalling typhoon pattern) are characterized by smaller coverage, shorter duration and stronger convection (larger coverage and longer duration). Both the synoptic patterns 1 and 2 are operating within the background large-scale EASM circulation featured by the strengthened WNPSH and accelerated low-level southwesterly winds. The landfalling typhoon pattern mainly occurs in August (>90% of the total landfalling typhoons in summer). Despite the landfalling typhoons only accounting for about 8% of the total summer RHEPE occurrences in the MLYRB, they account for ~50% of the total RHEPE occurrences in August.

Data Availability Statement

The hourly geopotential height, *u* and *v* component of wind speed, specific humidity and convective available potential energy data are accessed from ERA5 (Hersbach et al., 2020, available at https://doi.org/10.24381/cds.bd0915c6). All figures are made by NCAR Command Language (Version 6.4.0), which is available at https://www.ncl.ucar.edu/.

Acknowledgments
This work is supported by the National Key R&D Program of China under Grant 2022YFF0801601, the National Natural Science Foundation of China under Grant 41975081 and 42075020, the Open Grants of the State Key Laboratory of Severe Weather (2021LASW-A12), the Research Funds for the Frontiers Science Center for Critical Earth Material Cycling Nanjing University, the Fundamental Research Funds for the Central Universities (020914380103), the Jiangsu University "Blue Project" outstanding young teachers training object, and the Jiangsu Collaborative Innovation Center for Climate Change. We appreciate the High Performance Computing Center of Nanjing University for providing us the computing resource. We thank the editor and four reviewers for their constructive suggestions to greatly improve our manuscript.

References

Allen, M. R., & Ingram, W. J. (2002). Constraints on future changes in climate and the hydrologic cycle. *Nature*, *419*(6903), 228–232. https://doi.org/10.1038/nature01092

Berg, P., & Haerter, J. O. (2013). Unexpected increase in precipitation intensity with temperature—A result of mixing of precipitation types? *Atmospheric Research*, *119*(January), 56–61. https://doi.org/10.1016/j.atmosres.2011.05.012

Chen, G., Sha, W., & Iwasaki, T. (2009). Diurnal variation of precipitation over southeastern China: 2. Impact of the diurnal monsoon variability. *Journal of Geophysical Research*, *114*(D21), D21105. https://doi.org/10.1029/2009JD012181

Ding, Y. (2004). Seasonal March of the East-ASIAN summer monsoon (pp. 3–53). https://doi.org/10.1142/9789812701411_0001

Ding, Y., & Chan, J. C. L. (2005). The East Asian summer monsoon: An overview. *Meteorology and Atmospheric Physics*, *89*(1–4), 117–142. https://doi.org/10.1007/s00703-005-0125-z

Donat, M. G., Lowry, A. L., Alexander, L. V., O'Gorman, P. A., & Maher, N. (2016). More extreme precipitation in the world's dry and wet regions. *Nature Climate Change*, *6*(5), 508–513. https://doi.org/10.1038/nclimate2941

Du, Y., & Chen, G. (2018). Heavy rainfall associated with double low-level jets over southern China. Part I: Ensemble-based analysis. *Monthly Weather Review*, *146*(11), 3827–3844. https://doi.org/10.1175/MWR-D-18-0101.1

Gao, C., Li, G., Xu, B., & Li, X. (2020). Effect of spring soil moisture over the Indo-China Peninsula on the following summer extreme precipitation events over the Yangtze River basin. *Climate Dynamics*, *54*(9–10), 3845–3861. https://doi.org/10.1007/s00382-020-05187-5

Gocic, M., & Trajkovic, S. (2013). Analysis of changes in meteorological variables using Mann-Kendall and Sen's slope estimator statistical tests in Serbia. *Global and Planetary Change*, *100*, 172–182. https://doi.org/10.1016/j.gloplacha.2012.10.014

Gottardi, F., Obled, C., Gailhard, J., & Paquet, E. (2012). Statistical reanalysis of precipitation fields based on ground network data and weather patterns: Application over French mountains. *Journal of Hydrology*, *432–433*, 154–167. https://doi.org/10.1016/j.jhydrol.2012.02.014

Gu, D. (2019). Population division exposure and vulnerability to natural disasters for world's cities*. Retrieved from www.unpopulation.org

Gu, H., Yu, Z., Wang, G., Wang, J., Ju, Q., Yang, C., & Fan, C. (2015). Impact of climate change on hydrological extremes in the Yangtze River Basin, China. *Stochastic Environmental Research and Risk Assessment*, *29*(3), 693–707. https://doi.org/10.1007/s00477-014-0957-5

He, J., Ju, J., Wen, Z., Lü, J., & Jin, Q. (2007). A review of recent advances in research on Asian monsoon in China. *Advances in Atmospheric Sciences*, *24*(6), 972–992. https://doi.org/10.1007/s00376-007-0972-2

Hersbach, H., Bell, B., Berrisford, P., Hirahara, S., Horányi, A., Muñoz-Sabater, J., et al. (2020). The ERA5 global reanalysis. *Quarterly Journal of the Royal Meteorological Society*, *146*(730), 1999–2049. https://doi.org/10.1002/qj.3803

Hu, X., Ai, W., Qiao, J., Hu, S., Han, D., & Yan, W. (2022). Microphysics of summer precipitation over Yangtze-Huai river valley region in China revealed by GPM DPR observation. *Earth and Space Science*, *9*(3), e2021EA002021. https://doi.org/10.1029/2021EA002021

Hu, Y., Deng, Y., Lin, Y., Zhou, Z., Cui, C., & Dong, X. (2021). Dynamics of the spatiotemporal morphology of Mei-yu fronts: An initial survey. *Climate Dynamics*, *56*(9–10), 2715–2728. https://doi.org/10.1007/s00382-020-05619-2

Hu, Y., Deng, Y., Zhou, Z., Cui, C., & Dong, X. (2019). A statistical and dynamical characterization of large-scale circulation patterns associated with summer extreme precipitation over the middle reaches of Yangtze River. *Climate Dynamics*, *52*(9–10), 6213–6228. https://doi.org/10.1007/s00382-018-4501-z

Huang, D., Takahashi, M., & Zhang, Y. (2011). Analysis of the Baiu precipitation and associated circulations simulated by the MIROC coupled climate system model. *Journal of the Meteorological Society of Japanese Series II*, *89*(6), 625–636. https://doi.org/10.2151/jmsj.2011-603

Hui, P., Tang, J., Wang, S., & Wu, J. (2015). Sensitivity of simulated extreme precipitation and temperature to convective parameterization using RegCM3 in China. *Theoretical and Applied Climatology*, *122*(1–2), 315–335. https://doi.org/10.1007/s00704-014-1300-2

Jiang, X., Luo, Y., Zhang, D.-L., & Wu, M. (2020). Urbanization enhanced summertime extreme hourly precipitation over the Yangtze River delta. *Journal of Climate*, *33*(13), 5809–5826. https://doi.org/10.1175/JCLI-D-19-0884.1

Kamae, Y., Imada, Y., Kawase, H., & Mei, W. (2021). Atmospheric rivers bring more frequent and intense extreme rainfall events over east Asia under global warming. *Geophysical Research Letters*, *48*(24), e2021GL096030. https://doi.org/10.1029/2021GL096030

Kendon, E. J., Blenkinsop, S., & Fowler, H. J. (2018). When will we detect changes in short-duration precipitation extremes? *Journal of Climate*, *31*(7), 2945–2964. https://doi.org/10.1175/JCLI-D-17-0435.1

Li, H., Hu, Y., Zhou, Z., Peng, J., & Xu, X. (2018). Characteristic features of the evolution of a Meiyu frontal rainstorm with Doppler radar data assimilation. *Advances in Meteorology*, *2018*, 1–17. https://doi.org/10.1155/2018/9802360

Li, X., Zhang, K., Bao, H., & Zhang, H. (2022). Climatology and changes in hourly precipitation extremes over China during 1970–2018. *Science of the Total Environment*, *839*, 156297. https://doi.org/10.1016/j.scitotenv.2022.156297

Lin, L., Gettelman, A., Xu, Y., Wu, C., Wang, Z., Rosenbloom, N., et al. (2019). CAM6 simulation of mean and extreme precipitation over Asia: Sensitivity to upgraded physical parameterizations and higher horizontal resolution. *Geoscientific Model Development*, *12*(8), 3773–3793. https://doi.org/10.5194/gmd-12-3773-2019

Luo, N., & Guo, Y. (2021). Impact of model resolution on the simulation of precipitation extremes over China. *Sustainability*, *14*(1), 25. https://doi.org/10.3390/su14010025

Luo, Y., Wang, H., Zhang, R., Qian, W., & Luo, Z. (2013). Comparison of rainfall characteristics and convective properties of monsoon precipitation systems over south China and the Yangtze and Huai River Basin. *Journal of Climate*, *26*(1), 110–132. https://doi.org/10.1175/JCLI-D-12-00100.1

Luo, Y., Wu, M., Ren, F., Li, J., & Wong, W.-K. (2016). Synoptic situations of extreme hourly precipitation over China. *Journal of Climate*, *29*(24), 8703–8719. https://doi.org/10.1175/JCLI-D-16-0057.1

Luu, L. N., Vautard, R., Yiou, P., & Soubeyroux, J.-M. (2022). Evaluation of convection-permitting extreme precipitation simulations for the south of France. *Earth System Dynamics*, *13*(1), 687–702. https://doi.org/10.5194/esd-13-687-2022

Nayak, M. A., & Ghosh, S. (2013). Prediction of extreme rainfall event using weather pattern recognition and support vector machine classifier. *Theoretical and Applied Climatology*, *114*(3–4), 583–603. https://doi.org/10.1007/s00704-013-0867-3

Ng, C., Zhang, Q., & Li, W. (2021). Changes in hourly extreme precipitation over eastern China from 1970 to 2019 dominated by synoptic-scale precipitation. *Geophysical Research Letters*, *48*(5), e2020GL090620. https://doi.org/10.1029/2020GL090620

Nguyen-Le, D., & Yamada, T. J. (2019). Using weather pattern recognition to classify and predict summertime heavy rainfall occurrence over the Upper Nan River Basin, Northwestern Thailand. *Weather and Forecasting*, *34*(2), 345–360. https://doi.org/10.1175/WAF-D-18-0122.1

Nguyen-Le, D., Yamada, T. J., & Tran-Anh, D. (2017). Classification and forecast of heavy rainfall in northern Kyushu during Baiu season using weather pattern recognition. *Atmospheric Science Letters*, *18*(8), 324–329. https://doi.org/10.1002/asl.759

Ninomiya, K. (1984). Characteristics of Baiu front as a predominant subtropical front in the summer Northern Hemisphere. *Journal of the Meteorological Society of Japanese Series II*, *62*(6), 880–894. https://doi.org/10.2151/jmsj1965.62.6_880

Ninomiya, K. (2000). Large- and meso-α-scale characteristics of Meiyu/Baiu front associated with intense rainfalls in 1–10 July 1991. *Journal of the Meteorological Society of Japanese Series II*, *78*(2), 141–157. https://doi.org/10.2151/jmsj1965.78.2_141

O'Gorman, P. A., & Muller, C. J. (2010). How closely do changes in surface and column water vapor follow Clausius–Clapeyron scaling in climate change simulations? *Environmental Research Letters*, *5*(2), 025207. https://doi.org/10.1088/1748-9326/5/2/025207

Prein, A. F., Rasmussen, R. M., Ikeda, K., Liu, C., Clark, M. P., & Holland, G. J. (2017). The future intensification of hourly precipitation extremes. *Nature Climate Change*, *7*(1), 48–52. https://doi.org/10.1038/nclimate3168

Ren, X., Sha, Y., Shi, Z., & Liu, X. (2021). Response of summer extreme precipitation over East Asia during the mid-Holocene versus future global warming. *Global and Planetary Change*, *197*, 103398. https://doi.org/10.1016/j.gloplacha.2020.103398

Sun, B., Wang, H., Wang, A., Miao, Y., Zhou, B., & Li, H. (2021). Regularity and irregularity of the seasonal Northward march of the East Asian summer wet environment and the influential Factors. *Journal of Climate*, *34*(2), 545–566. https://doi.org/10.1175/JCLI-D-20-0333.1

Sun, Q., Zhang, X., Zwiers, F., Westra, S., & Alexander, L. V. (2021). A global, continental, and regional analysis of changes in extreme precipitation. *Journal of Climate*, *34*(1), 243–258. https://doi.org/10.1175/JCLI-D-19-0892.1

Tang, Y., Huang, A., Wu, P., Huang, D., Xue, D., & Wu, Y. (2021). Drivers of summer extreme precipitation events over east China. *Geophysical Research Letters*, *48*(11). https://doi.org/10.1029/2021GL093670

Thackeray, C. W., Hall, A., Norris, J., & Chen, D. (2022). Constraining the increased frequency of global precipitation extremes under warming. *Nature Climate Change*, *12*(5), 441–448. https://doi.org/10.1038/s41558-022-01329-1

Tian, F., Li, S., Dong, B., Klingaman, N. P., Freychet, N., & Sparrow, S. (2022). Physical processes of summer extreme rainfall interannual variability in eastern China: Part I—Observational analysis. *Climate Dynamics*, *59*(1–2), 201–217. https://doi.org/10.1007/s00382-021-06123-x

Tian, Y., Mcbride, J. L., Ren, F., Li, G., & Feng, T. (2022). Changes in typhoon regional heavy precipitation events over China from 1960 to 2018. *Advances in Atmospheric Sciences*, *39*(2), 272–283. https://doi.org/10.1007/s00376-021-1015-0

Tripathy, B. K., Anveshrithaa, S., & Ghela, S. (2021). Spectral clustering. In *Unsupervised learning approaches for dimensionality reduction and data visualization* (pp. 99–107). CRC Press. https://doi.org/10.1201/9781003190554-10

van de Vyver, H., van Schaeybroeck, B., De Troch, R., Hamdi, R., & Termonia, P. (2019). Modeling the scaling of short-duration precipitation extremes with temperature. *Earth and Space Science*, *6*(10), 2031–2041. https://doi.org/10.1029/2019EA000665

von Luxburg, U. (2007). A tutorial on spectral clustering. *Statistics and Computing*, *17*(4), 395–416. https://doi.org/10.1007/s11222-007-9033-z

Wei, S., Jian, L., & Ru-Cong, Y. (2013). Corresponding relation between warm season precipitation extremes and surface air temperature in south China. *Advances in Climate Change Research*, *4*(3), 160–165. https://doi.org/10.3724/SP.J.1248.2013.160

Wood, R. R., & Ludwig, R. (2020). Analyzing internal variability and forced response of subdaily and daily extreme precipitation over Europe. *Geophysical Research Letters*, *47*(17), e2020GL089300. https://doi.org/10.1029/2020GL089300

Xiao, C., Wu, P., Zhang, L., & Song, L. (2016). Robust increase in extreme summer rainfall intensity during the past four decades observed in China. *Scientific Reports*, *6*(1), 38506. https://doi.org/10.1038/srep38506

Xie, Z., Du, Y., Zeng, Y., & Miao, Q. (2018). Classification of yearly extreme precipitation events and associated flood risk in the Yangtze-Huaihe river valley. *Science China Earth Sciences*, *61*(9), 1341–1356. https://doi.org/10.1007/s11430-017-9212-8

Xue, M., Luo, X., Zhu, K., Sun, Z., & Fei, J. (2018). The controlling role of boundary layer inertial oscillations in Meiyu frontal precipitation and its diurnal cycles over China. *Journal of Geophysical Research: Atmospheres*, *123*(10), 5090–5115. https://doi.org/10.1029/2018JD028368

Yang, S., & Smith, E. A. (2006). Mechanisms for diurnal variability of global tropical rainfall observed from TRMM. *Journal of Climate*, *19*(20), 5190–5226. https://doi.org/10.1175/JCLI3883.1

Zhang, A. Q., Chen, Y. L., Zhou, S. N., Cui, C. G., Wan, R., & Fu, Y. F. (2020). Diurnal variation of Meiyu rainfall in the Yangtze plain during atypical Meiyu Years. *Journal of Geophysical Research: Atmospheres*, *125*(1), e2019JD031742. https://doi.org/10.1029/2019JD031742

Zhang, Q., Zheng, Y., Singh, V. P., Luo, M., & Xie, Z. (2017). Summer extreme precipitation in eastern China: Mechanisms and impacts. *Journal of Geophysical Research: Atmospheres*, *122*(5), 2766–2778. https://doi.org/10.1002/2016JD025913

Zhang, W., Furtado, K., Wu, P., Zhou, T., Chadwick, R., Marzin, C., et al. (2021). Increasing rainfall variability on daily-to-multiyear timescales. *Science Advances*, *7*(31), eabf8021. https://doi.org/10.1126/sciadv.abf8021

Zhang, W., & Zhou, T. (2020). Increasing impacts from extreme precipitation on population over China with global warming. *Science Bulletin*, *65*(3), 243–252. https://doi.org/10.1016/j.scib.2019.12.002

Zhao, C., Xu, M., Wang, Y., Zhang, M., Guo, J., Hu, Z., et al. (2019). Modeling extreme precipitation over east China with a global variable-resolution modeling framework (MPASv5.2): Impacts of resolution and physics. *Geoscientific Model Development*, *12*(7), 2707–2726. https://doi.org/10.5194/gmd-12-2707-2019

Zhao, Y., Huang, A., Kan, M., Dong, X., Yu, X., Wu, Y., et al. (2020). Characteristics of hourly extreme precipitation along the Yangtze River Basin, China during warm season. *Scientific Reports*, *10*(1), 5613. https://doi.org/10.1038/s41598-020-62535-5